Journal of Saudi Chemical Society (2018) **22**, 919–929

King Saud University

Journal of Saudi Chemical Society

www.ksu.edu.sa
www.sciencedirect.com

ORIGINAL ARTICLE

Synthesis of ultra-small platinum, palladium and gold nanoparticles by *Shewanella loihica* PV-4 electrochemically active biofilms and their enhanced catalytic activities

Elaf Ahmed, Shafeer Kalathil, Le Shi, Ohoud Alharbi, Peng Wang *

Water Desalination and Reuse Center, Division of Biological and Environmental Sciences and Engineering, King Abdullah University of Science and Technology, Thuwal, Saudi Arabia

Received 24 November 2017; revised 6 February 2018; accepted 8 February 2018
Available online 21 February 2018

KEYWORDS

Electrochemically active biofilm;
Ultra-small nanoparticles;
Shewanella loihica

Abstract Ultra-small nanoparticles (USNPs) of noble metals have a great potential in a variety of applications due to their high surface areas and high reactivity. This work employed electrochemically active biofilms (EABs) composed of a single bacterium strain of *Shewanella loihica* PV-4 and successfully synthesized USNPs of noble metal Au, Pd, and Pt. The synthesized USNPs had a size range between 2 and 7 nm and exhibited excellent catalytic performance in dye decomposition. The results of this work shine light on the use of EABs in nanoparticle synthesis.

1. Introduction

Ultra-small nanoparticles (USNPs), defined as a class of particles having size of 1–10 nm [1,2], due to their size, lie between complete molecular dispersions and large-sized nanoparticles (NPs) and accordingly reveal intermediate structural, optical [3], electrical [4], catalytic [5], and magnetic properties [6], often different from large NPs of the same material [1,2,7]. For example, noble metal USNPs, such as gold (Au), silver (Ag), palladium (Pd) and platinum (Pt) show attenuated surface plasmon resonance and exhibit molecular-like optical properties due to loss of their metallic properties [8–10].

USNPs have applications in diverse fields, including catalysis [11], photocatalysis [12,13], energy conversion and storage, chemical manufacturing, biological applications, biomedicines [14–21], semiconductors [22], and environmental treatments [14]. Especially, the catalytic activity of USNPs particularly of noble metals represents a rich resource for chemical processes [23,24].

There are a myriad of chemical synthesis methods available in literature to synthesize USNPs of noble metals, including reduction, thermal decomposition, and sol-gel processes [8,24–27]. However, all of them involve intensive use of chemical agents [8,10,28], making them environmentally unfriendly. Furthermore, the addition of surfactant, polymeric stabilizer, and other capping agents to stabilize these USNPs make the

* Corresponding author.
E-mail address: Peng.Wang@kaust.edu.sa (P. Wang).
Peer review under responsibility of King Saud University.

Production and hosting by Elsevier

https://doi.org/10.1016/j.jscs.2018.02.002

synthesis process complicated and severely limit the activity of these USNPs as catalysts [28–31].

Recently, biological approaches to nanoparticle synthesis using microorganisms, especially bacteria, offer certain attractions [32]. Over their evolution, bacteria have developed mechanisms which involve altering the chemical natures of some toxic metals to eliminate their toxicity and thus allow themselves to survive and grow properly [33]. This change in the chemical nature sometimes leads to formation of metal *nano*particles. Hence, the formation of the metal nanoparticles is literally an incidental by-product of a bacterial resistance mechanism against a specific metal, but has been gradually developed into an alternative way of purposefully producing nanoparticles [34].

In this regard, many microorganisms, such as bacteria, fungi, and yeast, have been exploited to synthesize metal nanoparticles [35]. Among these microorganisms, bacteria are typically favorable choices due to their abundant availability, ease of handling, easy genetic manipulation, and the fact that studies on one bacterium can be easily extrapolated to others [36,37].

Electrochemically active biofilm (EAB) is the biofilm that is grown on any artificial electrodes [38,39]. The utility and performance of EAB have been intensively studied in the past decades especially within microbial fuel cells (MFCs) systems to harvest energy from various environmental wastewater [40,41]. In the past decade, the use of EABs for purposeful nanoparticle synthesis and modification has grown considerably as the EAB-assisted nanoparticle synthesis involves less chemical usage and mild synthesis conditions that are amicable to biofilm residing bacteria [8,30,36,42,43]. Thus, EAB holds certain potential to be an emerging platform for metal nanoparticle synthesis in future. In literature, mixed bacterial cultures were extensively seen and used in metal nanoparticle synthesis while the use of a single strain bacteria was rarely investigated for the same purpose [35]. In this work, EAB composed of a single bacteria strain, *Shewanella loihica* PV-4, was cultivated and used so to investigate its capability of synthesizing UNSPs of noble metal. The results show that the EAB of *S. loihica* PV-4 leads to a successful synthesis of USNPs of Au, Pd, and Pt and the synthesized USNPs possess high catalytic activities toward degradation of a common dye. The results of this work show promising potential of single-strain EAB assisted USNP synthesis and thus invites more research efforts into this emerging field.

2. Experimental method and characterization

2.1. Biofilm preparation and growth

S. loihica PV-4 was obtained from the Deutsche Sammlung von Mikroorganismen und Zellkulturen (DSMZ) bacterium collection under the number DSM 17748. Literature conditions were used to grow the bacteria [44].

Commercial carbon paper was used as a support for the biofilm to grow on (Fuel cells ETC 6354706) and the carbon paper was cut into uniform pieces of (2 × 3 cm). The bioreactor for EAB growth, which was sealable 100 ml glass bottle, was first filled with 88 ml of the sterilized nutrient media, then 10 mM sodium lactate as an electron donor and 10 mM sodium fumarate as an electron acceptor. The solution was mixed very well to get a homogeneous mixture and the bioreactor was initially purged with nitrogen gas for 30 min to remove all the dissolved oxygen to maintain anaerobic conditions.

An aliquot of 10 ml of *S. loihica* PV-4 single strain inoculum with an optical density (OD) of 2 in nutrient media was then added to the bioreactor, followed by immediately putting the bioreactor inside a constant-temperature chamber of 30 °C. The carbon paper was quickly immersed into the media and the bottle was tightly sealed to ensure that there was no oxygen infused into the solution. The medium was continuously stirred for one week, by the end of which a living EAB would have been developed on the surface of the carbon paper as illustrated in Fig. 1. It is important to mention that there was no potential involved in the formation of the biofilm on the surface of the carbon paper.

The electrochemical activity of the EAB formed on the carbon paper was investigated using cyclic voltammetry (CV) measurement. The CV analysis was performed by Autolab Potentiostat, using a standard three-electrode system, with Ag/AgCl as the reference electrode, Pt mesh as the counter electrode and the EAB formed on the carbon paper as the working electrode. The artificial media, containing 10 mM sodium lactate was used as the electrolyte during the CV measurements. The scan rate used was 5 mV/S.

2.2. EAB-assisted synthesis of Au, Pd and Pt USNPs

Gold (III) chloride (99%, $AuCl_3$, Sigma-Aldrich), chloroplatinic acid (hydrate (≥99.9% trace metals basis $H_2PtCl_6{\cdot}xH_2O$, Sigma-Aldrich), palladium (II) chloride ($PdCl_2$ 99%, Sigma-Aldrich) were used as the precursors to Au, Pt, and Pd USNPs in this work.

The metal precursor solution of 1 mM was first prepared by using DI water and 10 mM sodium lactate as the electron donor within the glass bottle of the same dimension as the bioreactors in the previous step. The prepared precursor solution was purged with nitrogen gas for 30 min to ensure an anaerobic condition. To investigate the effect of pH on the nanoparticle synthesis, a set of the precursor solutions with different pH values of 4, 7 and 9 were prepared for each metal.

The carbon paper with the EAB prepared previously was then carefully transferred into the metal precursor solution reactor. The reactor was then tightly sealed and continuously stirred for 48 h in the constant temperature chamber of 30 °C.

After 48 h, the synthesized nanoparticles were collected by centrifuging the solution containing the particles at 13,500 RPM for 20 min. The supernatant was carefully emptied out and the precipitate solid was mixed with acetone for 5 min followed by centrifuging at 13,500 RPM for another 20 min. The supernatant was emptied out again and 10 ml of ethanol was used then to store the USNPs before use. Control experiments were conducted using the same metal precursor and sodium lactate in the absence of EAB to confirm the role of the EBA to produce the nanoparticles.

2.3. Dye degradation experiment

The as-synthesized Pd USNPs were tested for their catalytic activities to accelerate the degradation of a synthetic dye: methyl orange ($C_{14}H_{14}N_3NaO_3S$, Sigma-Aldrich). In conduct-

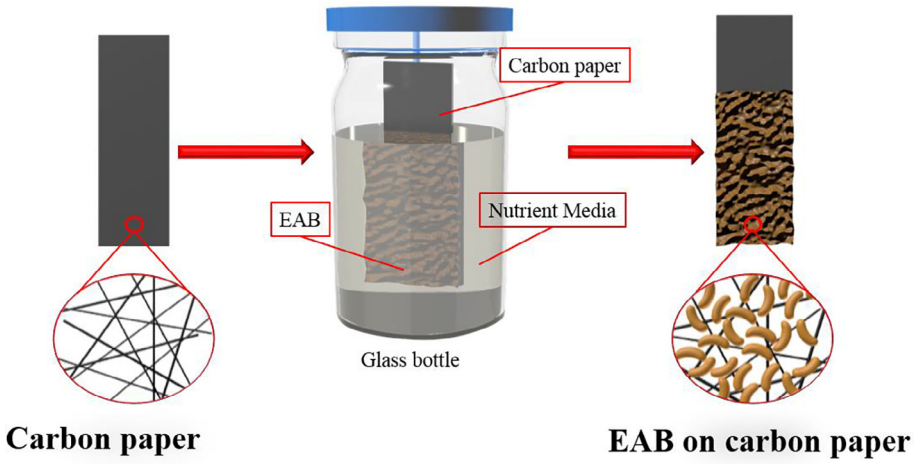

Fig. 1 Schematic growing procedure of EAB on the surface of a carbon paper.

ing dye degradation experiment, a 50 μL of the stock solution of methyl orange dye with 0.15 mM concentration was transferred to a 5 ml glass bottle, followed by adding 1.0 ml DI water. 100 μL sodium tetrahydridoborate ($NaBH_4$) with a concentration of 0.1 M was then added to the solution as reductant. An aliquot of 100 μL of the as the synthesized Pd USNPs (0.3 mg/mL) in ethanol solution was added to the prepared dye solution containing $NaBH_4$. An immediate color change was observed as soon as the metal nanoparticles were added to the dye solution. The dye concentration was measured by the UV–Vis absorbance at 468 nm.

2.4. Material characterizations

Scanning electron microscopy (SEM) (FEI Instruments) was used to characterize the surface morphology of the carbon paper and the carbon paper covered by the EAB. In conducting SEM observation, the sample was fixed using 3% of glutaraldehyde in cacodylate buffer (pH ~6.8) as a fixative. The fixation was done overnight to ensure a complete infiltration of the fixative into the sample matrix. Prior to SEM, samples were coated with a 4 nm thin layer of Pd/Pt metals using K575X sputter.

Transmission electron microscopy (TEM) was used to study the morphology, crystal structure, and the elemental distributions of the USNP samples. TEM analyses of the samples were performed using a TitanG2 80-300 CT from FEI Instruments that was equipped with a field-emission-gun and a GIF Tridiem 863 energy-filter from Gatan, Inc. Before the TEM analysis, the samples were prepared by diluting 250 μL of the nanoparticle solution in 750 μL ethanol then sonicated for 5 min to ensure the homogeneous solution and prevent any aggregation. Then the sample was placed on a copper grid for the TEM analysis.

The UV–Vis adsorption spectra were recorded on a spectrophotometer (Shimadzu, UV 2550), using DI water as a reference. X-ray diffraction (XRD) patterns were recorded on a Bruker D8 Advanced A25 diffractometer equipped with a Cu X-ray tube (Cu K_α; $\lambda = 0.154$ nm) operated at 40 kV and 40 mA from 30 to 80°.

3. Results and discussion

3.1. EAB characterizations

The *Shewanella* strains bacteria have attracted great attention because of their diverse respiratory capacities, illustrated by their ability to utilize a wide range of terminal electron acceptors, including oxygen, nitrate, metals and sulfur compounds, and also due to their confirmed extracellular electron transfer (EET) capability [38,45].

In this work, carbon paper was chosen as a support for the biofilm because of its mechanical stability, high electric conductivity, and biocompatibility, low cost and wide availability. Fig. 2a presents SEM images of the plain carbon paper. As can be seen, the carbon paper has an interwoven fiber structure with a uniform fiber diameter around 10 μm and a smooth surface. The visual change on the surface of the carbon paper before and after the growth of the biofilms was very significant. It can be clearly seen that there was a sticky pinkish layer grown on the carbon paper fibers with a total coverage of the surface after seven days biofilm growth and the layer represented the EAB as shown in Fig. S1.

From Fig. 2b–d, it can be clearly seen that there was a total coverage of the bacteria cells on the surface of the carbon paper and each fiber of the paper was fully wrap-covered. These are good signs showing that the bacteria in the EAB were in healthy conditions. The bacteria in the EAB were condense and formed a thick layer with individual bacteria in close contact to one another and being very well connected. Some free bacterial cells could be located and from these bacteria the size and the structure of the bacteria were recognized. The length of the individual bacteria is around 1–3 μm and diameter of 0.8 μm, which is very well consistent with the literature as shown in Fig. S2 [46,47].

Cyclic voltammetry (CV), a type of potential sweep method, is probably the most widely used analytical tool for examining the EET process in EABs for detecting the activity of EABs. Although in this work, the Ag/AgCl reference electrode was used in the measurement, for the convenience of comparison, all the potential were converted to be relative to reversible hydrogen electrode (RHE) using Eq. (1).

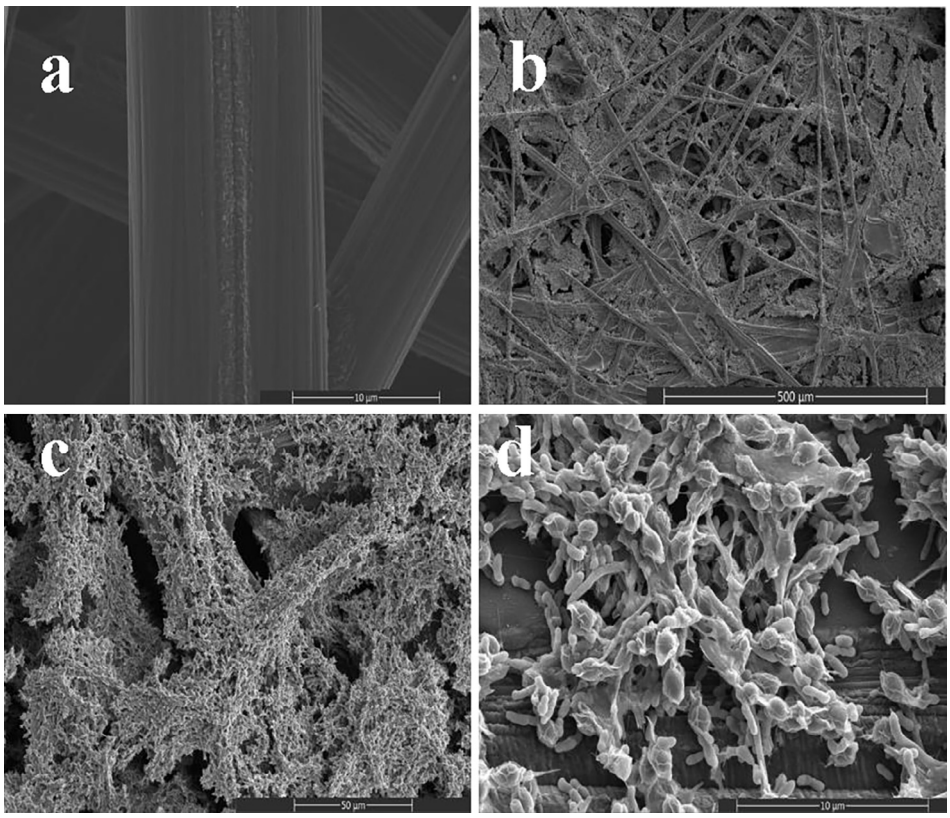

Fig. 2 (a) SEM images of plain carbon paper, (b–d) and EAB grown on the surface of carbon paper at different magnifications.

$$E_{RHE} = E_{Ag/Agcl} + 0.059pH + E^{\circ}_{Ag/Agcl} \quad (1)$$

where E_{RHE} is the converted potential vs. RHE, $E^{\circ}_{Ag/AgCl}$ = 0.1976 at 25 °C, and $E_{Ag/AgCl}$ is the experimentally measured potential against Ag/AgCl reference electrode.

The CV measurements were conducted with EAB formed on the carbon paper as the working electrode immersed with artificial media containing 10 mM sodium lactate as the electrolyte. Fig. 3 compares the EAB grown for different time courses, 0, 1, 4, and 7 days.

From the results in Fig. 3, it can be noted that by increasing the duration of the EAB growth, the recorded current was increased. The EAB grown for 7 days period, produced the highest negative current among all samples under the same conditions. The results can be explained by the fact that EAB gown in 7 days had the highest population of bacteria in the biofilm. The bacteria grown on the carbon paper responded to the applied potential and increased the produced current. Among all samples, the plain carbon paper shows the lowest current response and this is due to the lack of bacterial

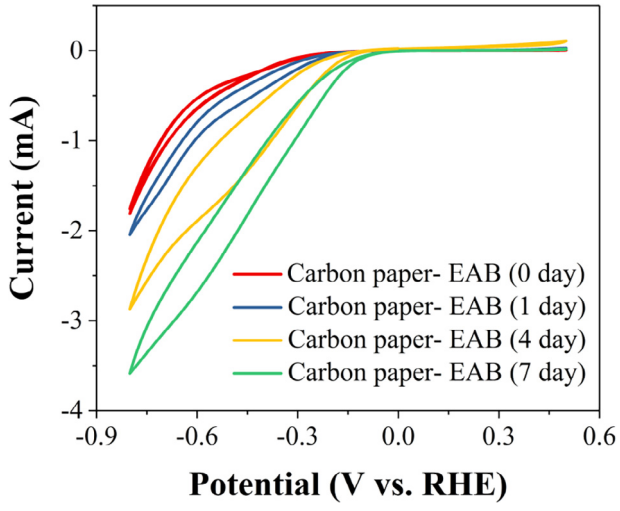

Fig. 3 Cyclic voltammetry plots of carbon paper and EAB formed carbon paper with a scan rate of 5 mV/S.

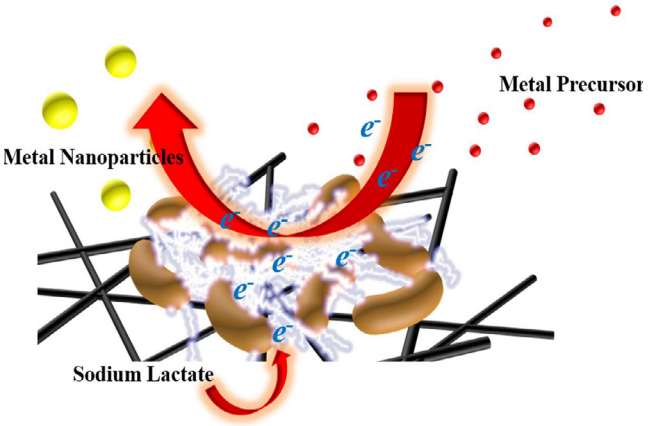

Fig. 4 Schematic illustration of the synthesis of UNSPs by EAB.

cells on its surface. Thus, the positive relationship between the electrochemical responses of the EABs and their growth duration implies reactivity and viability of the biofilms on the carbon paper.

The electrochemically active bacteria present in the EAB would biologically oxidize sodium lactate (electron donor) and produces extracellular electrons. Electrochemically active bacteria have the capability to transfer electrons extracellularly through different mechanisms: direct electron transfer (DET) and mediated electron transfer (MET) mechanisms [47]. It has been reported that electrochemically active bacteria have self-secreted mediators such as Flavin. These mediators have the ability to carry electrons from the bacterial cell to the external acceptor in the media [48,49].

Electrons are a strong reducing agent, which can then reduce metal precursors that are present abundantly in the surrounding media to produce nanoparticles as illustrated in Fig. 4. In the following sections, the effects of pH and metal precursor concentrations on the USNP formation are investigated.

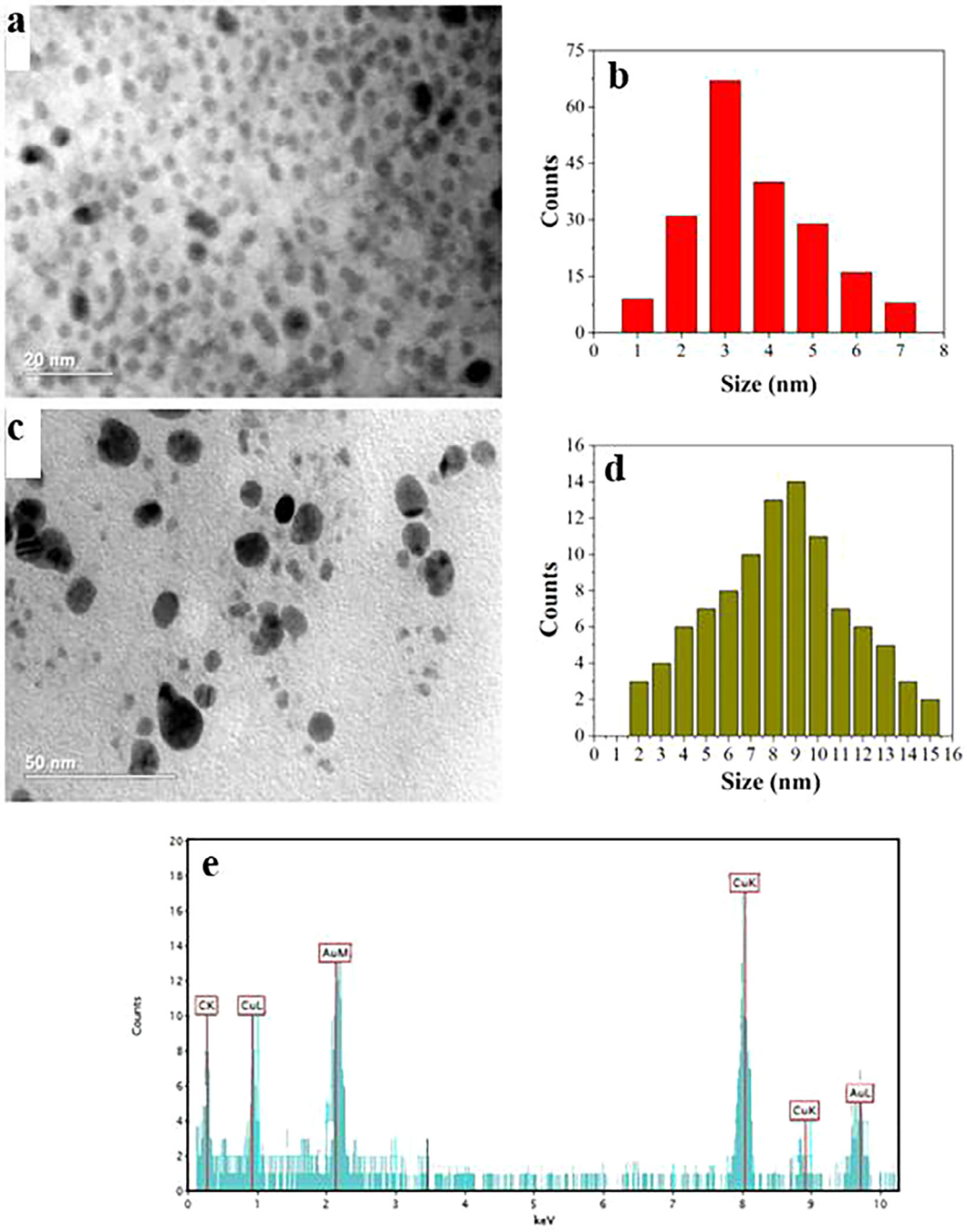

Fig. 5 TEM image (a) and particle size distribution (b) of as-synthesized Au NPs at pH 7; TEM image (c) and particle size distribution (d) of as-synthesized Au NPs at pH 9; (e) EDX spectra of the Au NPs.

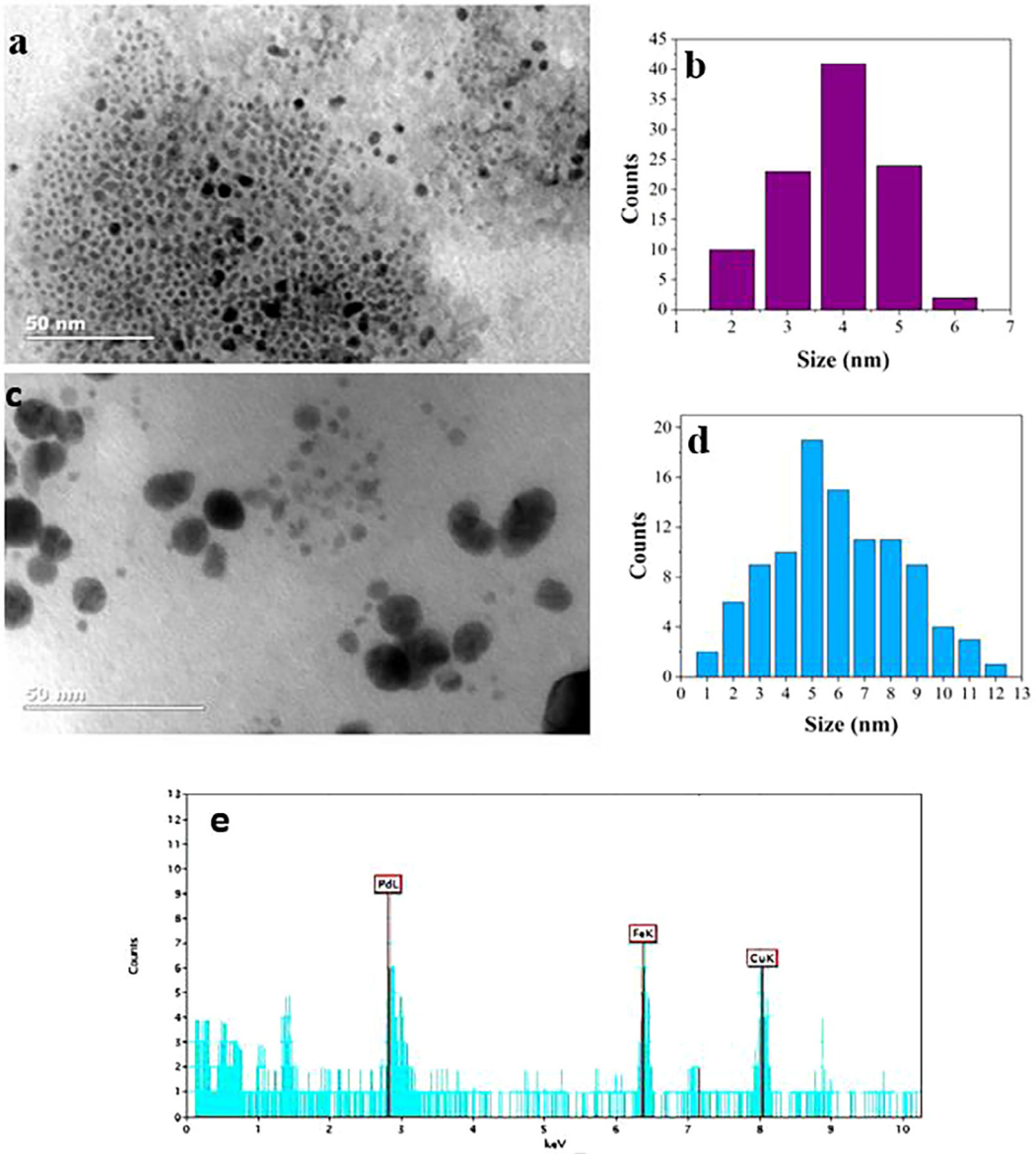

Fig. 6 TEM image (a) and particle size distribution (b) of as-synthesized Pd NPs at pH 7; TEM image (c) and particle size distribution (d) of as-synthesized Pd NPs at pH 9; (e) EDX spectra of the Pd NPs.

3.2. Effect of pH the USNP formation

In studying the effect of the pH on the USNP synthesis, three different pHs, namely 4, 7, 9 of the metal precursor solutions with precursor concentration fixed at 1 mM were tested. It was quickly found that at pH 4, there was no production of metal nanoparticles due to the intolerance of *S. loihica* PV-4 to the acidic medium of pH 4. Fig. S3 shows SEM images of dead *S. loihica* PV-4 cells after placing the carbon paper with living biofilm in the precursor solution of pH 4 for 48 h. Some damaged and ruptured cell structures are clearly seen, which confirms that the EAB poorly responded to acidic conditions and that the biofilm was factor in unsuccessful synthesis of nanoparticles at pH 4. In the cases with pH 7 and 9, successful nanoparticle synthesis was obtained.

Fig. 5a and c presents the TEM of Au nanoparticles synthesized at pH 7 and pH 9. As can be seen, the produced particles were fairly uniform and had a size of USNPs ranging between 2 and 7 nm in the case of pH 7 and 2–15 nm in pH 9. Fig. 5b and d shows the size distribution histogram of the synthesized Au USNPs, which was manually measured from TEM images with more than 100 particles. EDX spectrum in Fig. 5e clearly confirms that these nanoparticles were Au. The successful production of Au USNPs confirms the role of the EAB in the experiments as well as the effect of pH value.

Fig. 6a and b present TEM images and size distribution histogram of the synthesized Pd nanoparticles at pH 7. The produced Pd nanoparticles were fairly uniform and had a size of USNPs ranging between 2 and 6 nm. At pH 9, the USNPs of Pd were also produced with slightly bigger size ranging 2–12 nm as shown in Fig. 6c and d. Fig. 6e confirms the USNPs

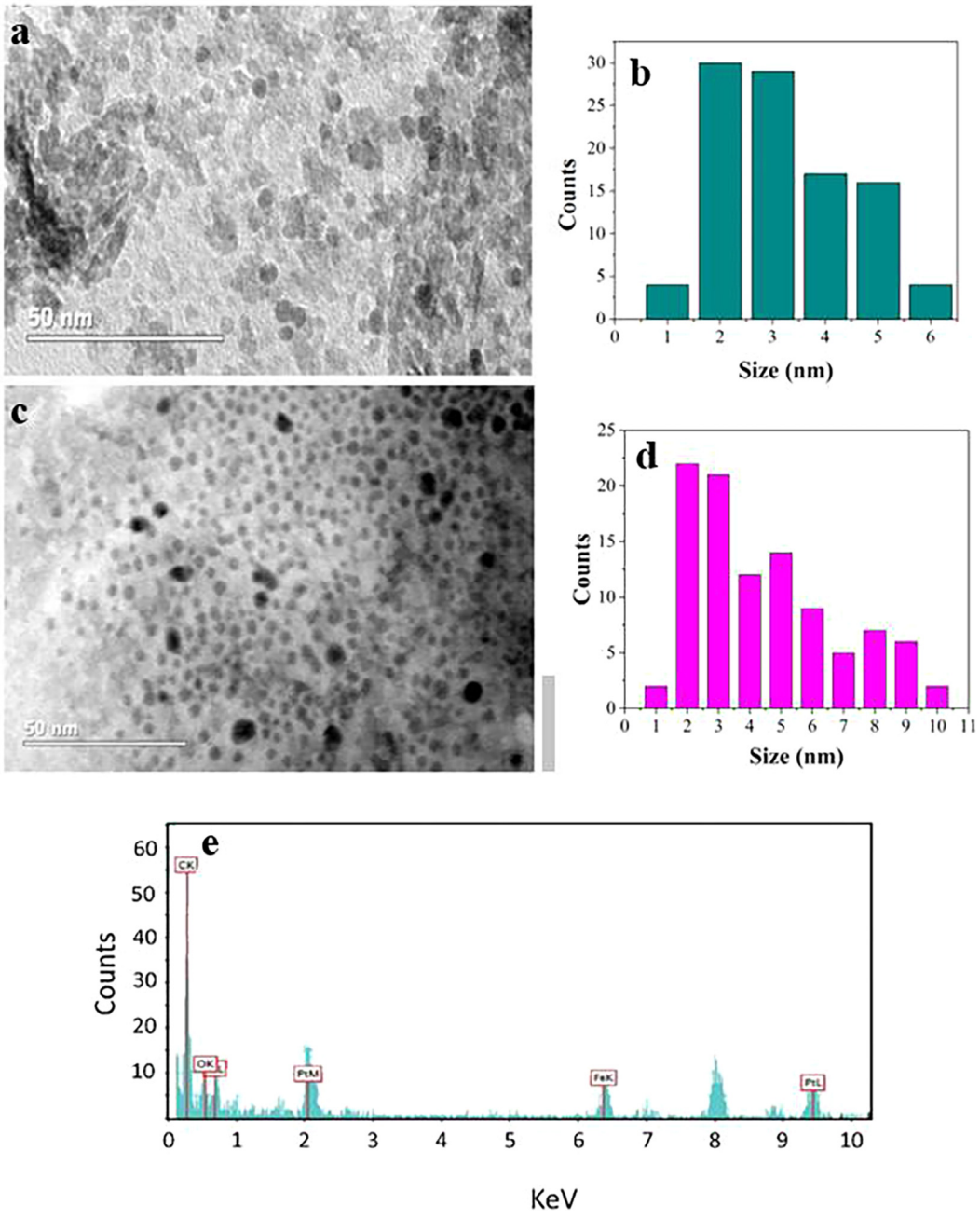

Fig. 7 TEM image (a) and particle size distribution (b) of as-synthesized Pt NPs at pH 7; TEM image (c) and particle size distribution (d) of as-synthesized Pt NPs at pH 9; (e) EDX spectra of the Pt NPs.

being Pd using EDX spectra. For Pt, at pH 7 the produced nanoparticles were uniform with sizes of 2–6 nm (Fig. 7a and b). At pH 9, the USNPs of Pt were also successfully produced with the size between 2 and 10 nm (Fig. 7c and d). EDX spectra confirm that the particles were Pt NPs in Fig. 7e.

Thus, when pH is either 7 or 9, relatively uniform USNPs of all three metal, Au, Pd, and Pt were successfully synthesized and the sizes of the particles fell into the range of USNPs with good size distribution, with the size range at pH 9 a bit wider than that at pH 7. The above results confirm successful production of USNPs of noble metals by EAB.

3.3. Effect of metal precursor concentrations on the USNP formation

To study the effect of concentrations of the metal precursors on the formation of the nanoparticles, four concentrations of metal precursors were investigated for each metal, 0.1, 0.5, 1.0 and 5.0 mM. In all cases, the concentrations of 0.1 mM of three metal precursor solutions failed to produce any particles while, in comparison, with the concentrations being increased to 0.5, 1 and 5.0 mM, the USNPs were successfully formed as shown in the TEM images Fig. 8. For all of these

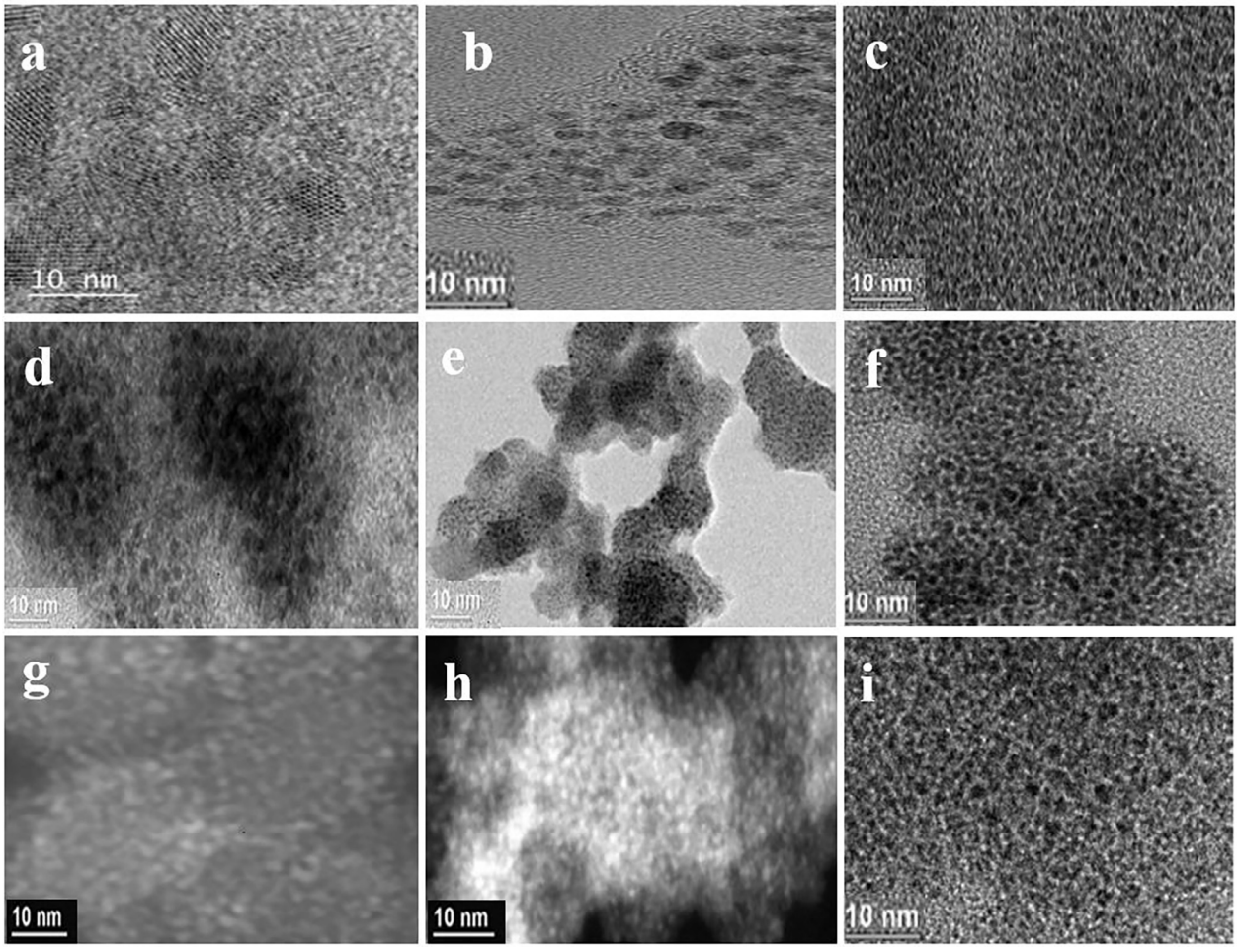

Fig. 8 TEM images of (a–c) Pd NPs synthesized with the precursor concentration of (a) 0.5 mM, (b) 1 mM and (c) 5 mM; (d–f) Pt USNPs synthesized with the precursor concentration of (d) 0.5 mM, (e) 1 mM and (f) 5 mM; (g–i) Au USNPs synthesized with the precursor concentration of (g) 0.5 mM, (h) 1 mM and (i) 5 mM.

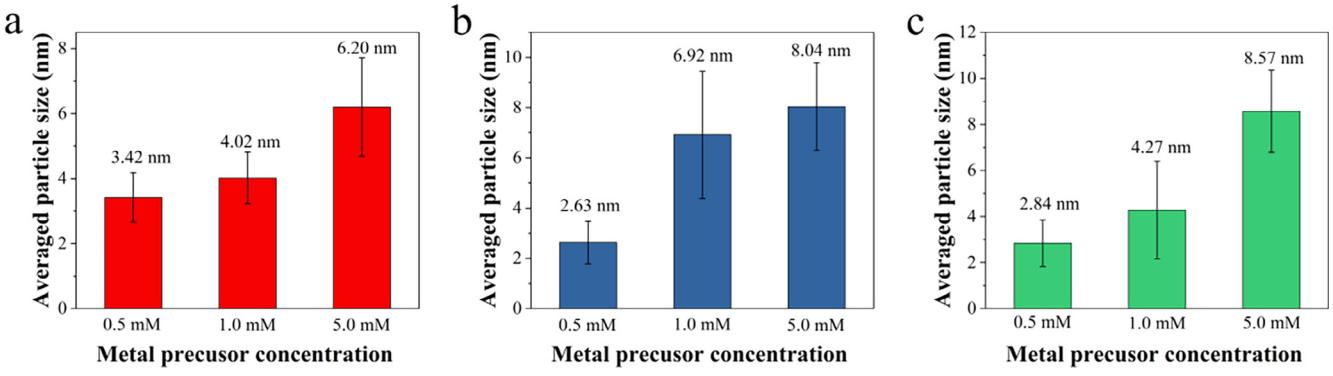

Fig. 9 The average sizes of the USNPs with different precursor concentrations (a) Au, (b) Pd, and (c) Pt NPs.

three metals, no large metal particles (> 20 nm) were observed, indicating this is a quite robust synthesis method for ultra-small noble metals.

Fig. 8a shows an HRTEM image for the Pd nanoparticles synthesis from 0.5 mM precursor. It clearly shows that each particle is highly crystalized with single crystalline nature. The interplanar spacing values measured from the HRTEM agree well with the theoretical values calculated from the crystal cell parameters of Pd [50].

Fig. 8b and c shows an HRTEM image for the Pd nanoparticles synthesized from 1.0 mM and 5.0 mM precursor. No obvious difference can be directly found. However, the statistically average particle sizes are varied for them with the same evolution trend. As the concentration of the precursor

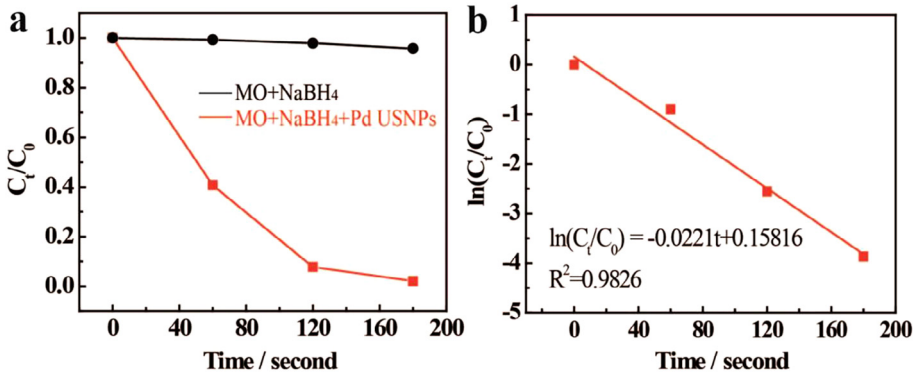

Fig. 10 (a) MO dye degradation using Pd USNPs, (b) Plot of $\ln(C_t/C_0)$ versus time for the reduction of MO using Pd USNPs.

increased, the average particle size of the products slightly increased in all three metal cases. For example, the average particle size was 2.62, 6.92 and 8.03 nm when the concentration of the precursor was 0.5, 1.0 and 5.0 mM for Pd NPs (Fig. 9a).

Fig. 8d–f, shows HRTEM images of the Pt nanoparticles synthesized at 0.5, 1.0 and 5.0 mM precursor solutions. As can be seen, USNPs were formed at all concentrations, with the average particle size being 2.84, 4.27 and 8.57 nm for 0.5, 1.0 and 5 mM respectively (Fig. 9b). The Au NPs show the same trend as the other two noble metals. Fig. 8g–I presents the TEM images of the Au NPs and their average particle size was 3.42, 4.02 and 6.19 nm for the 0.5, 1.0 and 5.0 mM precursor concentrations respectively Fig. 9c.

The clear relationship in all three metal cases between their precursor concentrations and their particle sizes provides an easy approach to control the average particle size during EAB-assisted noble metal nanoparticles. The XRD further confirms the crystallinity of the synthesized USNPs as shown in Fig. S4.

A control experiment was conducted in this work, where the otherwise same reaction was run separately to produce USNPs of the metals in the absence of the EAB. This test was conducted to ensure that the EAB is responsible for the formation of USNPs. As expected, the growth of USNPs in the reactor was unsuccessful in the absence of EAB.

In summary, the USNPs produced using *S. loihica* PV-4 had ultra-small size of 2–7 nm with the optimized pH and precursor concentration. When comparing the species of *Shewanella* with other bacteria, it is found that *Shewanella* tends to produce nanoparticles smaller than those produced by other microorganisms as reported in the literature. For example, *Pseudomonas stutzeri* reportedly produced metal nanoparticles with particle size around 46 nm while *Lactobacillus sp*., *Bacillus licheniformis*, and *Verticillium sp*. produced nanoparticles of 20, 50, and 25 nm respectively [51]. Presumably, the smaller particle size may be attributed to the higher reduction ability of *Shewanella* comparing to other bacteria.

3.4. Dye degradation performance by the UNSPs

Dye degradation experiments were performed to test the effect of the produced USNPs. In this experiment the Pd USNPs produced at pH 7 were collected and used as a catalyst for methyl orange (MO) degradation.

As a control, with only $NaBH_4$ being in the MO solution, no noticeable degradation occurred during the experiment as shown in Fig. S5. As can be seen from Fig. 10, using Pd USNPs in the presence of $NaBH_4$ shows an instant MO degradation. As a matter of a fact, Pd USNPs exhibited excellent catalytic performances in MO degradation. The degradation of MO using USNPs took around 50 s to see a drastic color change of the solution. Fig. 10b shows that the MO degradation in this case follows the first-order kinetics.

4. Conclusion

In this work, EAB of *S. loihica* PV-4 was employed to successfully synthesize USNPs of Au, Pd and Pt. This synthesis method involves mild operating conditions, consumes less chemicals, and is more environmentally friendly. The synthesized USNPs all show good catalytic activity on the degradation of methyl orange dye. This work shines light on the use of EAB for effective and controllable synthesis of USNPs.

Acknowledgements

This work was supported by the King Abdullah University of Science and Technology (KAUST) center competitive fund (CCF) awarded to Water Desalination and Reuse Center (WDRC). The authors are grateful to the other members of the KAUST Environmental Nanotechnology group for the helpful discussions.

Appendix A. Supplementary data

Supplementary data associated with this article can be found, in the online version, at https://doi.org/10.1016/j.jscs.2018.02.002.

References

[1] K. Ma et al, Controlling growth of ultrasmall sub-10 nm fluorescent mesoporous silica nanoparticles, Chem. Mater. 25 (5) (2013) 677–691.
[2] K. Ma, H. Sai, U. Wiesner, Ultrasmall sub-10 nm near-infrared fluorescent mesoporous silica nanoparticles, J. Am. Chem. Soc. 134 (32) (2012) 13180–13183.

[3] K.L. Kelly et al, The optical properties of metal nanoparticles: the influence of size, shape, and dielectric environment, J. Phys. Chem. B 107 (3) (2003) 668–677.
[4] V. Aleksandrovic et al, Preparation and electrical properties of Cobalt−Platinum nanoparticle monolayers deposited by the Langmuir−Blodgett technique, ACS Nano 2 (6) (2008) 1123–1130.
[5] A. Mohanty, N. Garg, R. Jin, A universal approach to the synthesis of noble metal nanodendrites and their catalytic properties, Angew. Chem. Int. Ed. 49 (29) (2010) 4962–4966.
[6] J. Tuček et al, Air-stable superparamagnetic metal nanoparticles entrapped in graphene oxide matrix, Nat. Commun. 7 (2016) 12879.
[7] L. Boselli et al, Regimes of biomolecular ultrasmall nanoparticle interactions, Angew. Chem. Int. Ed. 56 (15) (2017) 4215–4218.
[8] B.H. Kim et al, Synthesis, characterization, and application of ultrasmall nanoparticles, Chem. Mater. 26 (1) (2013) 59–71.
[9] R. Dong et al, Towards ultra small noble metal nanoparticles: testing Jellium model for ligand protected copper and silver M 13 core nanoparticles, PCCP 13 (8) (2011) 3274–3280.
[10] S. Iravani, Bacteria in nanoparticle synthesis: current status and future prospects, Int. Scholarly Res. Not. 2014 (2014) 18.
[11] F. Wang et al, Porous single-crystalline palladium nanoparticles with high catalytic activities, Angew. Chem. Int. Ed. 51 (20) (2012) 4872–4876.
[12] M.E. Khan, M.M. Khan, M.H. Cho, Green synthesis, photocatalytic and photoelectrochemical performance of an Au-Graphene nanocomposite, RSC Adv. 5 (34) (2015) 26897–26904.
[13] M.E. Khan, M.M. Khan, M.H. Cho, Biogenic synthesis of a Ag–graphene nanocomposite with efficient photocatalytic degradation, electrical conductivity and photoelectrochemical performance, New J. Chem. 39 (10) (2015) 8121–8129.
[14] K.E. Drexler, Nanotechnology: from Feynman to funding, Bull. Sci. Technol. Soc. 24 (1) (2004) 21–27.
[15] K. Huang et al, Size-dependent localization and penetration of ultrasmall gold nanoparticles in cancer cells, multicellular spheroids, and tumors in vivo, ACS Nano 6 (5) (2012) 4483–4493.
[16] L. Dykman, N. Khlebtsov, Gold nanoparticles in biomedical applications: recent advances and perspectives, Chem. Soc. Rev. 41 (6) (2012) 2256–2282.
[17] S. Huo et al, Ultrasmall gold nanoparticles as carriers for nucleus-based gene therapy due to size-dependent nuclear entry, ACS Nano 8 (6) (2014) 5852–5862.
[18] C. Sun, J.S. Lee, M. Zhang, Magnetic nanoparticles in MR imaging and drug delivery, Adv. Drug Deliv. Rev. 60 (11) (2008) 1252–1265.
[19] O. Veiseh, J.W. Gunn, M. Zhang, Design and fabrication of magnetic nanoparticles for targeted drug delivery and imaging, Adv. Drug Deliv. Rev. 62 (3) (2010) 284–304.
[20] O.C. Farokhzad, R. Langer, Impact of nanotechnology on drug delivery, ACS Nano 3 (1) (2009) 16–20.
[21] R. Costo et al, Ultrasmall iron oxide nanoparticles for biomedical applications: improving the colloidal and magnetic properties, Langmuir 28 (1) (2011) 178–185.
[22] A. Dawson, P.V. Kamat, Semiconductor–metal nanocomposites. Photoinduced fusion and photocatalysis of gold-capped TiO_2 (TiO_2/Gold) Nanoparticles, J. Phys. Chem. B 105 (5) (2001) 960–966.
[23] L. Zhang, W. Niu, G. Xu, Synthesis and applications of noble metal nanocrystals with high-energy facets, Nano Today 7 (6) (2012) 586–605.
[24] Z. Fan, H. Zhang, Template synthesis of noble metal nanocrystals with unusual crystal structures and their catalytic applications, Acc. Chem. Res. 49 (12) (2016) 2841–2850.
[25] C. Wang et al, A general approach to the size-and shape-controlled synthesis of platinum nanoparticles and their catalytic reduction of oxygen, Angew. Chem. Int. Ed. 47 (19) (2008) 3588–3591.
[26] S. Shankar et al, Green synthesis of silver nanoribbons from waste X-ray films using alkaline protease, Mater. Express 5 (2) (2015) 165–170.
[27] S. Xu et al, Ultrasmall organic nanoparticles with aggregation-induced emission and enhanced quantum yield for fluorescence cell imaging, Anal. Chem. 88 (15) (2016) 7853–7857.
[28] S. Babu Kalidindi, U. Sanyal, B.R. Jagirdar, Chemical synthesis of metal nanoparticles using amine–boranes, ChemSusChem 4 (3) (2011) 317–324.
[29] M.M. Khan et al, Synthesis of cysteine capped silver nanoparticles by electrochemically active biofilm and their antibacterial activities, Bull. Korean Chem. Soc. 33 (8) (2012) 2592–2596.
[30] S. Dulon et al, Electroactive biofilms: new means for electrochemistry, J. Appl. Electrochem. 37 (1) (2007) 173–179.
[31] S.-J. Chiu et al, Versatile synthesis of thiol-and amine-bifunctionalized silica nanoparticles based on the ouzo effect, Langmuir 30 (26) (2014) 7676–7686.
[32] X. Li et al, Biosynthesis of nanoparticles by microorganisms and their applications, J. Nanomater. 2011 (2011) 16.
[33] A.O. Olaniran, A. Balgobind, B. Pillay, Bioavailability of heavy metals in soil: impact on microbial biodegradation of organic compounds and possible improvement strategies, Int. J. Mol. Sci. 14 (5) (2013) 10197–10228.
[34] N. Pantidos, L.E. Horsfall, Biological synthesis of metallic nanoparticles by bacteria, fungi and plants, J. Nanomed. Nanotechnol. 5 (5) (2014) 1.
[35] S. Kalathil et al, Production of bioelectricity, bio-hydrogen, high value chemicals and bioinspired nanomaterials by electrochemically active biofilms, Biotechnol. Adv. 31 (6) (2013) 915–924.
[36] S. Kalathil, J. Lee, M.H. Cho, Electrochemically active biofilm-mediated synthesis of silver nanoparticles in water, Green Chem. 13 (6) (2011) 1482–1485.
[37] P.L. Tremblay, L.T. Angenent, T. Zhang, Extracellular electron uptake: among autotrophs and mediated by surfaces, Trends Biotechnol. 35 (4) (2017) 360–371.
[38] J. Babauta et al, Electrochemically active biofilms: facts and fiction. A review, Biofouling 28 (8) (2012) 789–812.
[39] M.M. Khan et al, Mixed culture electrochemically active biofilms and their microscopic and spectroelectrochemical studies, ACS Sustainable Chem. Eng. 2 (3) (2013) 423–432.
[40] P. Pandey et al, Recent advances in the use of different substrates in microbial fuel cells toward wastewater treatment and simultaneous energy recovery, Appl. Energy 168 (2016) 706–723.
[41] S. Bajracharya et al, An overview on emerging bioelectrochemical systems (BESs): technology for sustainable electricity, waste remediation, resource recovery, chemical production and beyond, Renewable Energy 98 (2016) 153–170.
[42] M.M. Khan, Bioenergy derived from electrochemically active biofilms, in: Biomass and Bioenergy, Springer, 2014, pp. 79–88.
[43] E.C. Salas et al, Reduction of graphene oxide via bacterial respiration, ACS Nano 4 (8) (2010) 4852–4856.
[44] Y. Roh et al, Metal reduction and iron biomineralization by a psychrotolerant Fe(III)-reducing bacterium, *Shewanella* sp. strain PV-4, Appl. Environ. Microbiol. 72 (5) (2006) 3236–3244.
[45] N.J. Kotloski, J.A. Gralnick, Flavin electron shuttles dominate extracellular electron transfer by *Shewanella oneidensis*, MBio 4 (1) (2013) e00553–e612.
[46] H. Gao et al, *Shewanella loihica* sp. nov., isolated from iron-rich microbial mats in the Pacific Ocean, Int. J. Syst. Evol. Microbiol. 56 (8) (2006) 1911–1916.
[47] A. Jain et al, Electron transfer mechanism in *Shewanella loihica* PV-4 biofilms formed at graphite electrode, Bioelectrochemistry 87 (2012) 28–32.

[48] L. Shi et al, Extracellular electron transfer mechanisms between microorganisms and minerals, Nat. Rev. Microbiol. 14 (2016) 651.
[49] S. Kalathil, D. Pant, Nanotechnology to rescue bacterial bidirectional extracellular electron transfer in bioelectrochemical systems, RSC Adv. 6 (36) (2016) 30582–30597.
[50] K. Koh et al, Ultrasmall palladium nanoparticles supported on amine-functionalized SBA-15 efficiently catalyze hydrogen evolution from formic acid, J. Mater. Chem. A 2 (48) (2014) 20444–20449.
[51] M.M. Khan et al, Novel Ag@TiO_2 nanocomposite synthesized by electrochemically active biofilm for nonenzymatic hydrogen peroxide sensor, Mater. Sci. Eng. C 33 (8) (2013) 4692–4699.